Manipulating Standard and Inverse Chladni Patterns by Modulating Adhesive, Frictional, and Damping Forces

Mohit Shridhar

October 11, 2011

Abstract

Particles on a plate form Chladni patterns when the plate is acoustically excited. To better understand these patterns and their possible real-world applications, I present a new analytical and numerical study of the transition between standard and inverse Chladni patterns on an adhesive surface at any magnitude of acceleration. By spatial autocorrelation analysis, I examine the effects of surface adhesion and friction on the rate of pattern formation. Next, I explore displacement models of particles translating on a frictional surface with both adhesive and internal particle-plate frictions. In addition, I find that both adhesion and damping forces serve as exquisite particle sorting mechanisms. Finally, I discuss the possible real-world applications of these sorting mechanisms, such as separating nanoparticles, organelles, or cells.

Contents

1 Introduction

In 1787, Ernst Chladni showed that sand particles on an acoustically excited metal plate rearrange themselves into esthetic patterns [1]. Ever since, researchers have been using Chladni patterns to study standing waves and other harmonic behaviors [2]. The resonance of a horizontal plate deflects the sand particles away from the antinodes of the vibration, leading to the formation of patterns at the nodes. Recently, experiments on inverse Chladni patterns [3, 4] (i.e., particles collecting at the antinodes of an oscillating plate) have revealed a new area of research. In addition, both nodal and antinodal Chladni patterns have been observed in microparticles and nanoparticles [5]; these patterns effectively position and sort such particles.

In this study, I examine the effects of adhesion, friction, and damping on the development of Chladni patterns, and suggest real-world applications for these effects. It has been showed that by manipulating the vibrational acceleration of the plate around the critical value g, it is possible to switch between nodal and antinodal patterns [3]. In my simulations, I replicate this effect using adhesion. This study also explains the mechanics of the particle sorting process, which can be controlled by adhesion and damping. In addition, I use spatial autocorrelation analysis to explore the effects of adhesion and frictional forces on the rate of pattern formation. Primarily, I present analytical explanations of these phenomena, and then verify them with numerical simulations.

1.1 Dynamics of an oscillating plate

For centuries, researchers have attempted to develop a model to predict Chladni patterns. Several attempts were based on deriving a relationship between the number of diametric (linear) nodes and the frequency of oscillation [6]. To create more accurate models, researchers analyzed the mathematics of the vibrating plate instead of directly studying the nodal regions [7, 8]. The vertical deflection function of an acoustically excited plate oscillated to one of its natural resonant frequencies ω_{kl} corresponds to the integral count of the sinusoidal half wavelengths in the x-direction k and y-direction l:

$$z(x, y, t) = a\,sin(\omega_{kl}t)\,sin\frac{k\pi x}{L_x}\,sin\frac{l\pi y}{L_y}, \tag{1}$$

where a is the amplitude, L_x is the length of the plate and L_y is its width.

1.2 Inverse Chladni patterns

Despite the popularity of standard Chladni patterns, inverse Chladni patterns are relatively obscure. Gerner et al. has analyzed and numerically simulated the conditions for particles to collect at the antinodes, forming *Inverse* Chladni patterns [3]. Conventionally, inverse Chladni patterns were assumed to be induced by only small particles that were carried through air currents [9, 10, 11, 12]. However, Gerner et al. showed that when the vibrational acceleration of the plate is below g, the particles stop bouncing and remain in contact with the surface [3]. As a consequence, the particles translate

toward the antinodes irrespective of the influence of air currents. They also discussed the experimental constraints of producing inverse Chladni patterns: the structure of the plate must be perfectly horizontal, and a minimum frictional force is required to start the particles in a rolling motion [3]. The acceleration of a particle (from its center of mass) moving toward the antinode at a given time t is $a_{cm}(x, y, t) = W_{\parallel}(x, y, t)/$m, where $W_{\parallel}$ is the parallel weight of the particle relative to the surface.

1.3 Spatial autocorrelation analysis

Spatial autocorrelation is a geographical tool used to analyze a variable's degree of dependence on its proximal locations. A typical method of quantifying a pattern's spatial autocorrelation is to calculate its *Moran's I* value. A Moran's I value close to +1.0 indicates clustering and that close to –1.0 indicates dispersion [13]; a Moran's I value equal to 0 indicates pure randomness, i.e., no spatial autocorrelation. In this study, for analyzing the effect of adhesive and frictional forces on Chladni patterns, spatial autocorrelation values are used to quantify the amount of particle clustering caused by accelerations and other forces acting on the particles. Next, the effect of these forces on the rate at which patterns form is analyzed using Moran's I values.

1.3.1 Limitations of Moran's I values

All numerical simulations that were analyzed for spatial autocorrelation involved particles initially positioned in a grid-like structure before the plate was allowed to oscillate. Hence, hypothetically, as patterns start to form, the Moran's I value should gradually increase. However, Moran's I values do not indicate whether the patterns are in standard or inverse form. These values also do not represent the degree of similarity between the subject pattern and the nodal lines of the vibrating plate. In other words, Moran's I values do not measure how similar a pattern is to the ideal Chladni pattern that could be formed under such conditions.

2 Numerical Simulations

The numerical simulations consisted of a dynamic mesh, whose form was based on Eq. 1 at a given natural frequency and time. Spherical particles of 5 cm diameter and 1 kg mass were used instead of dust particles; large size and mass of particles were chosen to disprove the previous assumption that inverse patterns form only with small dust particles. To accommodate these large particles, the dimensions of the plate were set as $L_x = L_y = 10m$. The number of particles varied from 225 to 10,000. The particles were positioned in a grid-like structure (e.g. 100×100) on the resting position of the plate at $t = 0$. Numerical computing software packages MATLAB and Mathematica were used to simulate the dynamics of the oscillating mesh [14], and an external physics engine was used to calculate the body dynamics. The physics engine was optimized for particle–particle and particle–plate collisions.

2.1 Limitations and impractical elements of the numerical simulations

The simulated plate is completely horizontal; therefore, it does not contain any pre-made deformations, unlike a real plate. In addition, despite the massive 1 kg particles and the extensive area of the plate in these simulations, neither the plate's position nor its acceleration is affected in any manner by particle–plate collisions or by its own weight. Furthermore, these simulations contained the following: oscillating plates with dimensions of 10m × 10m, perfectly uniform surface adhesion, internal friction, and damping coefficients. The particles used in the simulations were also perfectly spherical and identical in size. Virtual experiments were performed in a vacuum to eliminate the effect of air currents on the particles. Because of the technical and financial constraints of controlling the conditions mentioned above, numerical simulations were performed instead of experiments.

The effects of two types of friction, sliding and rolling frictions, on the formation of inverse Chladni patterns are studied here. However, for conciseness and simplicity, only sliding friction is used in the numerical simulations. In later sections, I analytically explore the effects of both of these forces.

3 Rate of Pattern Formation

Chladni patterns have mostly been studied after the particles have formed a clear, definite shape. The rate of Chladni pattern formation reflects the influences of the forces acting on the particles. Thus, to determine the rate of pattern formation, I use spatial autocorrelation analysis as a quantifiable measure of the amount of particle clustering; this then allows me to attain an overview of the effects of adhesive and frictional forces.

3.1 Effects of adhesion

Figure 1 shows the effect of adhesion on the clustering of particles that were initially in a dispersed position (100 × 100 grid). The break-off force ($F_{N,Z}$) is the minimum amount of force required to eject a particle from the surface of the plate as a result of its acceleration. Uniform increments in $F_{N,Z}$, resulted in a steady increase in the initial rate of clustering; however, note that spatial autocorrelation analysis does not account for the number of particles involved in the clustering or for the number of slow-moving and stationary particles. The patterns were also found to quickly settle within a certain range of Moran's I values. At lower values of $F_{N,Z}$, particle movements are more chaotic, because the adhesive force has only a limited effect on them; therefore, the Moran's I values are closer to 0. At higher values of $F_{N,Z}$, particle movements are highly constricted, because the adhesive force has a strong effect on them; therefore, the Moran's I values are farther from 0 (in the positive direction).
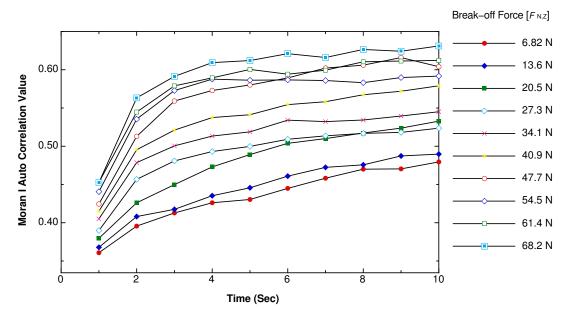
Figure 1: Effect of *adhesion* on the rate of pattern formation: Moran's I values of patterns formed from 1 to 10 s for various values of the break-off force (simulation parameters: $\mu_i = 0.1$, $f = 9$ Hz, and 10,000 particles).

3.2 Effects of friction

Figure 2 shows the effect of friction on the clustering of particles that were initially in a dispersed position (100×100 grid). The effect of friction is only applicable to sliding or rolling particles (in this case, sliding particles); therefore, the results in Fig. 2 were produced under complete inverse Chladni pattern conditions, where no particles were ejected from the surface because of the acceleration of the plate. $F_{N,Z}$ was kept constant at 6.82N, and the coefficient of internal particle–plate friction (i.e., the Coulomb friction coefficient) was uniformly increased from 0.1 to 0.8. The results obtained from the simulation differed slightly from those obtained from the adhesion control test. The Moran's I values at $t = 1s$ were almost identical for all values of μ_i, and the settling values were delayed until particles formed compact structures at the antinodes. The acceleration of the particles decreased as the frictional force increased; consequently, the rate of clustering was inversely proportional to μ_i.

4 Internal and Adhesive Friction

In this section, I examine the combined effects of adhesion and internal friction on the surface-parallel displacement of the particles. The internal frictional force, F_f is the resisting force acting against a sliding particle on a surface. Two types of friction are studied here: sliding and rolling frictions (the latter is studied only analytically).
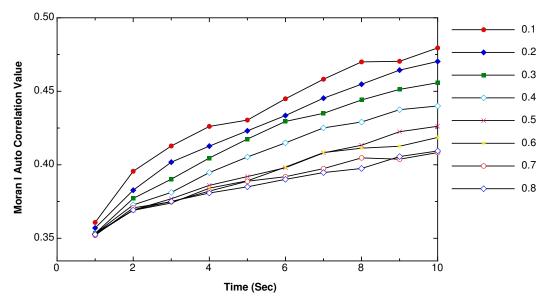
Figure 2: Effect of *friction* on the rate of pattern formation: Moran's I values of patterns formed from 1 to 10 s for various values of the Coulomb friction coefficient (simulation parameters: $F_{N,Z} = 6.82$N, $f = 9$ Hz and 10,000 particles).

4.1 Theory

First, we need to look at the forces that cause particles to translate on an oscillating surface. For all particles in contact with the vibrating surface, the vertical position at any given point can be derived from Eq. 1. Using the second derivative of Eq. 1, we can find the vertical acceleration of particles at any given time:

$$\ddot{z}(x, y, t) = a\omega_{kl}^2 \, sin(\omega_{kl}t) \, sin\frac{k\pi x}{L_x} \, sin\frac{l\pi y}{L_y}. \tag{2}$$

By adding the particles' acceleration due to gravity g to Eq. 2, it is possible to obtain the vertical weight W for a given mass m:

$$W(x, y, t) = -m\Big[g - \ddot{z}(x, y, t)\Big] = -m\left[g - a\omega_{kl}^2 \, sin(\omega_{kl}t) \, sin\frac{k\pi x}{L_x} \, sin\frac{l\pi y}{L_y}\right]. \tag{3}$$

Because of the dynamic nature of the plate, particles are subjected to plate-parallel $W_{\parallel}$ and plate-perpendicular $W_{\perp}$ forces (Fig. 3), which are partial components of the W vector.

Next, we must determine plate-parallel and frictional forces. To calculate $W_{\parallel}$ we need to know the slope of the plate for $z(x, y, t)$. This can be obtained by multiplying
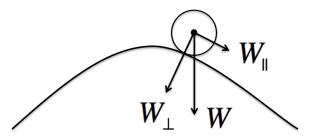
7

Figure 3: Weight W of a particle and its components ($W_\parallel$ and $W_\perp$) when it is in contact with a surface.

W with the gradient of Eq. 1:

$$W_\parallel(x,y,t) = W(x,y,t) \frac{dz(x,y,t)}{dx} \frac{dz(x,y,t)}{dy} \frac{dz(x,y,t)}{dt}. \tag{4}$$

The frictional force F_f acting against $W_\parallel$ is the combined effect of the adhesive force and the internal particle-plate friction. This combined effect was studied by Tomas [15], and the frictional force acting against a sliding particle was found to be:

$$F_f = \mu_i[F_N + F_H(F_N)], \tag{5}$$

where μ_i is the Coulomb friction coefficient, F_N is the normal force acting perpendicularly to the plate, and F_H is the adhesive force at (x,y,t). Although it is possible to calculate F_N directly by using the gradient function in Eq. 4, for simplicity I use $F_N = -W_\perp = -[W(x,y,t) - W_\parallel(x,y,t)]$, because it involves simple vector addition. During the oscillations, the adhesive force counteracts with force exerted by the plate; this force due to acceleration F_{acc} is dynamic and is given as $\approx -F_H = -W$; however, this is only true for $W < F_{N,Z}$, where $F_{N,Z}$ is the break-off force; thus particles are ejected if this limit is exceeded [16]. In addition, the rolling friction can be calculated in a similar manner [15]:

$$F_f = \mu_r[F_N + F_H(F_N)], \tag{6}$$

where we substitute the rolling friction coefficient μ_r for μ_i.

Now that we have formulated plate-parallel and frictional forces, we can combine them to determine the surface-parallel acceleration of a particle. For a given particle of mass m, its acceleration (from its center of mass) a_{cm} is given by $W_\parallel(x,y,t)/m$. Therefore, its acceleration after implementing the sliding frictional force is:

$$a_{cm} = \frac{W_\parallel(x,y,t) - \mu_i[F_N + F_H(F_N)]}{m}. \tag{7}$$

Similarly, the rolling friction can be calculated by replacing μ_i with μ_r.

4.2 Particle displacement: Numerical simulation

To confirm Eq. 7, a numerical simulation was performed (see Fig. 4). A 1×1 mode was setup at $\omega_{kl} = \frac{\sqrt{2}}{2}$ (one of the natural frequencies). The average surface-parallel acceleration of the particles over a complete cycle was calculated by integrating Eq. 7 from 0 to $2\pi/\omega_{kl}$. Then, the average acceleration was used to predict the position of the particles after 8 s.
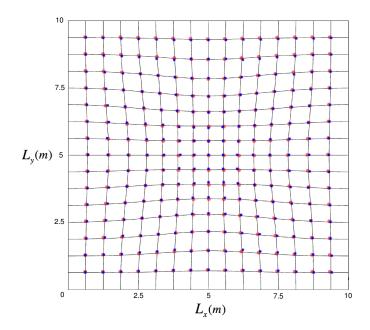

Figure 4: Particle displacement for $\mu_i = 0.1$. The red dots at the points of intersection in the 17×17 grid show the positions of particles predicted using Eq. 7 after 8 s. The blue dots show the positions of particles obtained from the numerical simulation.

The correlation between the predicted and simulated positions is very good. However, a few particles slightly deviated from their predicted positions. This is possibly due to the limitations of the simulator. The simulator's physics engine treats the plate as a dynamic mesh and breaks the area into a 14×14 grid to optimize the computational speed. Therefore, as the number of particles increases above 14×14, the precision of their positions decreases.

5   Adhesive Forces

So far, I have explored the frictional effects of adhesion. Now, I directly examine the contact forces acting between the plate and the particles. Oscillatory methods of measuring the break-off force (due to adhesion) have been previously reported [16]. The concept is similar to the dynamics of stress-based removal of particles from a surface (pulling a particle away from the plate), except that in oscillations, the pulling stress is

provided by the acceleration of the plate.

5.1 Particle ejection area

From the previous section, we have seen that F_{acc} is given as $\approx -F_{\text{H}} = -W(x,y,t)$, where F_{H} (for $W < F_{\text{N,Z}}$) acts in the same direction as W. This effect is also responsible for keeping the particles in contact with the plate. For all regions on the plate with $F_{acc} > F_{\text{N,Z}}$, the resultant force ejects the particles away from the plate; for all regions with $F_{acc} \leq F_{\text{N,Z}}$, the particles stay in contact with the surface. Therefore, an inequality can be derived to express the area (A_E) where the particles are ejected:

$$A_E = -W(x,y,t) - F_{\text{N,Z}} > 0. \tag{8}$$

5.2 Area-based sorting: Numerical simulation

A numerical simulation (see Fig. 5) was performed to confirm Eq. 8. The 1×1 mode setup from Section 4.2 was replicated, and a total of 2,500 particles were used. The friction coefficient of the surface was set to its maximum. Because of the ejection mechanism and the high friction coefficient, only particles in the ejection area (red in Fig. 5) will bounce off the plate; particles in the contact area (light blue in Fig. 5) will have no displacement, because they are restricted to neither bounce nor slide as a result of the strong adhesive and frictional forces acting on them. The boundary formed between the ejection area and the contact area in the numerical simulation accurately delineates the particle ejection area.

Experimentally replicating this simulation is challenging, because it is difficult to simultaneously achieve a low adhesive break-off force and a high frictional force. However, at substantial accelerations and frictional coefficients, it is possible to sustain a slow translation of particles in the contact area that allows enough time to completely eject all particles in the ejection area, which leads to an effective area-based sorting mechanism. This concept corresponds to the results of the spatial autocorrelation analysis where the particles' movements become less chaotic as $F_{\text{N,Z}}$ increased. Note that an increase in $F_{\text{N,Z}}$ causes the ejection area to decrease (Eq. 8); thus, more particles are constricted to surface-parallel translation and subjected to a stronger resistive frictional force. As a result of the increased resistive force, the particle movements are less chaotic, which leads to higher Moran's I values.
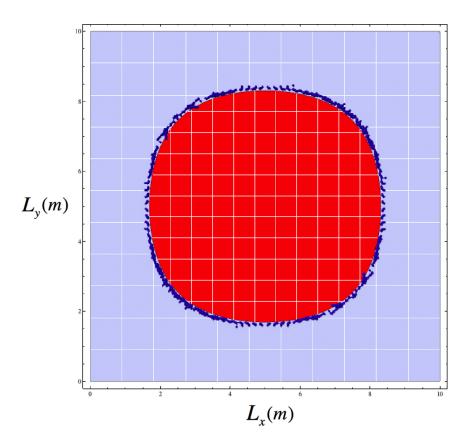
Figure 5: Particle ejection area (red). The blue dots surrounding the red area show the particle positions obtained from the numerical simulation. Stationary particles in the light blue region were ignored in the figure.

5.3 Using adhesion as a substitute for gravity

Gerner et al. switched between standard and inverse Chladni patterns by manipulating the acceleration of the plate [3]. Switching between these two types of patterns can also be achieved by applying uniform adhesion across the surface. In the acceleration-based control method, the critical value for shifting between the two types of patterns was determined by g, which is the acceleration due to gravity. In actual experiments, controlling the break-off force $F_{N,Z}$ due to adhesion might be more preferable than controlling g, because it provides more technical flexibility. However, uniform adhesion across the surface must be maintained; otherwise, some particles might not follow Eq. 8. The numerical simulations shown in Figs. 6a and 6b were performed under identical conditions, except that the surfaces had different $F_{N,Z}$ values. The critical $F_{N,Z}$ value that enables alternating between standard and inverse Chladni patterns can be determined by $F_{N,Z\,\text{critical}} = \Gamma m$, where Γ is the peak acceleration of the plate ($\Gamma = a\omega^2$) and m is the particle mass. Figure 6 clearly shows the effects of setting the break-off force value below and above its critical value.
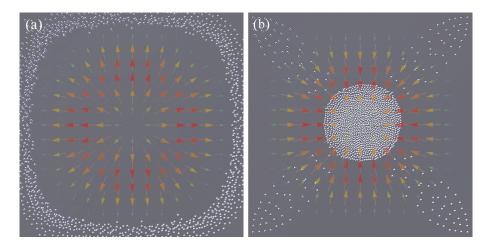
11

Figure 6: Using adhesion to alternate between standard and inverse Chladni patterns. The position of particles is shown at $t = 100$ s. (a) $F_{N,Z} = 1$N standard pattern of collection at the nodes. (b) $F_{N,Z} = 50$N inverse pattern of collection at the antinodes. Simulation parameters: 1×1 mode, 10,000 particles, $\omega_{kl} = \frac{\sqrt{2}}{2}$ and $\Gamma m = F_{N,Z\,\text{critical}} = 19.74$N.

5.4 Inverse Chladni patterns due to surface contact

To understand the reason for the particles to move toward the antinodes when $F_{acc} < F_{N,Z}$, we must understand the relation between gravity and adhesion. Let us consider a scenario where g is the critical value. If the vibrational acceleration of the plate is lower than g, at some points in the cycle, particles will accelerate upward, thus $|W| > mg$; at other points in the cycle, particles will accelerate downwards, thus $|W| < mg$. If this variation in $|W|$ is averaged over the cycle, the direction of the resultant force is toward the antinodes. In the case of adhesion, the adhesive force can be thought of as a substitute for the gravitational force: it pulls the particles down and keeps them in contact with the plate. Therefore, whenever a particle is in contact with the oscillating surface, a consistent force is applied toward the antinodes. Furthermore, this effect occurs regardless of the force responsible for maintaining surface contact. For further proof of this effect, I calculate the plate-parallel force $W_{\parallel}$ on the particles as the plate's acceleration a (given by Eq. 7) approaches infinity as follows:

$$\lim_{a \to \infty} W_{\parallel}(x, y, t) = m\omega^2 \sin(\omega t)\, k\pi x \, \sin\left[\frac{l\pi y}{L_y}\right]. \tag{9}$$

Gravity has been ignored for simplicity. Note that Eq. 9 always gives a positive value of $W_{\parallel}$, which indicates that the particles move toward the antinodes. Figure 7 is a vector plot indicating the direction of the particles' acceleration for Eq. 9. As indicated by the arrows, the particles move toward the antinodes even under extreme circumstances. Note that this effect occurs only when particles are in contact with the surface. However, in reality, at extreme accelerations the particles will be forcibly ejected from the surface
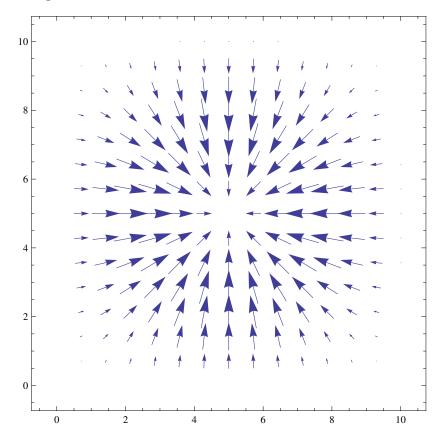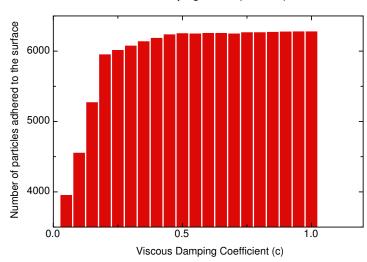
12

instead of sliding on it.

Figure 7: Direction of the particles' acceleration when in contact with the oscillating surface as the plate's acceleration approaches infinity. Simulation parameters: 1×1 mode produced on a $10(\mathrm{m}) \times 10(\mathrm{m})$ plate.

6 Viscous Damping

Damping is a form of friction that reduces the amplitude of an oscillation. However, in the case of Chladni patterns, damping does not affect sliding or rolling particles. In this study, damping refers to viscous damping caused by the surface chemistries of the plate and particles; it does not refer to frictional damping affecting the oscillation of the plate. The damping force exerted during a particle–plate collision can be modeled with $F_\mathrm{d} = -cv$, where c is the viscous damping coefficient and v is the velocity of the particle before the collision. For bouncing particles, it is very difficult to predict v; therefore, I study only the direct effects of the coefficient c, and do not calculate the damping force involved in collisions.

6.1 Particles in contact with the surface

When a bouncing particle hits a vibrating plate, the particle's resulting velocity depends on the velocity of the plate (upon impact), the particle's velocity before collision, and the viscous damping coefficient. Increasing the viscous damping coefficient proportionally reduces the resulting particle velocity by absorbing more of the force applied by the oscillating plate. If there is sufficient damping force, i.e., the break-off force is greater than the applied force, then the particle will not bounce at all, and instead it will temporarily stick to the surface (if the surface is uniformly adhesive) until the force exerted by the plate (later, at a certain point during the oscillation) is greater than the break-off force including the effect of viscous damping.

Effect of Damping at 3 Hz (t = 5 sec)

Figure 8: Effect of damping on the number of particles adhered to the surface. Both temporarily attached and permanently attached particles (due to adhesion and damping) were included in the count. The simulation was initiated with 10,000 particles. Other particles from the y-axis count either bounced (they were temporarily ejected) or were completely ejected from plate. Simulation parameters: $F_{\mathrm{N,Z}} = 6.82\mathrm{N}$, and $\mu_i = 0.1$.

Figure 8 presents the results of a simulation performed at $\omega_{kl} = 3\,\mathrm{Hz}$. The number of particles adhered to the surface at $t = 5s$ drastically increased with c up to 0.2; however, in the range $0.2 < c \leq 1.0$, the count either increased by a minute amount or remainded unchanged. At high damping coefficients, most of the particles remain in contact with the surface and cluster at the antinodes. In addition, high damping forces also reduce the number of particles that are completely ejected from the plate. To summarize, damping does not directly affect the type of Chladni pattern formed; however, it is a contributing factor in keeping the particles in contact with the surface, which (as seen in Section 5.4) is crucial for inducing inverse Chladni patterns.

14

6.2 Particle damping as a sorting mechanism

In Section 5.2, I explored how adhesion can be used as an area-based sorting mechanism. Similarly, particle damping can be used as a sorting mechanism. Thus far, I have studied the effect of the plate-damping force on bouncing particles. Now, I study the effect of the particle-damping force: the particle itself absorbs the collision energy through mechanical properties such as elasticity. If a particle system contains groups of particles with unique particle-damping coefficients, then this concept can be exploited to sort the particles into sets of similar kind. To verify this concept, a numerical simulation was performed with three different particle groups each having a different value of the particle-damping coefficient (Fig. 9a).
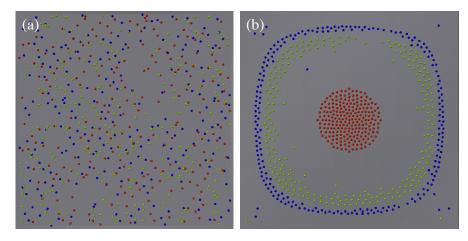

Figure 9: Numerical simulation of a sorting mechanism based on the particle-damping coefficient c. The particles had the following values of c: 0.1 (blue), 0.5 (green), and 0.9 (red). (a) Initial random positions of the particles. (b) Positions of the particles after 150 s

As seen in Fig. 9b, the particles were effectively sorted based on the value of their particle-damping coefficients. At lower values of the particle-damping coefficient, the particles tend to cluster closer to the nodes, whereas at higher values, the particles tend to cluster closer to the antinodes. Note that this trend is quantitatively nonlinear: an increase in the value of c from 0.1 (blue) to 0.5 (green) resulted in a small change in the cluster's position, whereas a proportionate increase in the value of c from 0.5 (green) to 0.9 (red) resulted in a large change in the cluster's position.

To understand how this sorting mechanism works, we need to look at the two forces that might act on a particle: the force on a bouncing particle due to the acceleration of the plate and the resultant force on a particle in contact with the surface due to the plate's average acceleration. These two forces can act simultaneously only if the surface contains a definite ejection area (Section 5.1). Furthermore, these two forces are also responsible for determining the position of the cluster. By changing the particle-damping coefficient, the boundary between the ejection area and the contact area can be

15

manipulated. This effect is illustrated in Fig. 10; the increase in the ejection area (light blue) from Fig. 10a to Fig. 10b is a direct result of the decrease in the particles' damping coefficients. At high particle-damping coefficients, the particles absorb more of the force exerted by the plate (F_{acc}). Here the damping force F_{d} opposing F_{acc} is sufficient to prevent the particles from bouncing (i.e., ejection), even if the particles reside in the ejection area (some regions only). Therefore, Eq. 8 becomes

$$A_E = -W(x, y, t) + F_{\mathrm{d}} - F_{\mathrm{N,Z}} > 0. \tag{10}$$

The increase of F_{d} in Eq. 8 results in a smaller ejection area, and . In contrast, the contact area (red regions in Fig. 10) of particles increases; hence, the particles move closer to the antinodes.
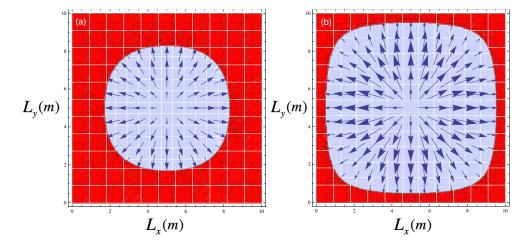

Figure 10: The effect of particle damping on the force (blue vectors) exerted on a bouncing particle within the ejection area (light blue). a) Forces experienced by particles with high damping coefficients. (b) Forces experienced by particles with low damping coefficients. These vector plots are just illustrations, and the difference between the ejection areas has been exaggerated; this figure is used only for qualitative analysis.

6.3   Limitations of the particle-damping based sorting system

This sorting mechanism lacks efficiency: as seen in Fig. 9b, not all particles have been sorted into their groups. As the particles translate, they collide with their own kind (e.g., two blue particles collide) and others (e.g., a blue particle collides with a red one). Under some circumstances, it is possible for particles to get fixated between clusters formed by other particles. The particle-damping dynamics in the simulations were based solely on mathematical models of damping properties; however, for real-world applications, mechanical properties such as deformation and elasticity must be carefully studied. In an experiment, the damping coefficient can be related to the elasticity of the particles, where energy is dissipated through temporary compression. The temporary compression

of a particle results in a spring action (rapid expansion) when the force compressing it changes direction; however, some of the energy is lost during the compression and expansion in the form of heat. More elastic materials will expand and contract in greater amounts; hence, hysteresis will increase, thereby dissipating more heat (although the difference might be exceptionally small), and thus, they are more likely to remain in contact with the surface. Therefore, a sorting mechanism experiment will result in a small difference between the cluster positions of particle groups when compared to the elegant delineations seen in Fig. 9b. Finally, an experiment would need to take into account the external forces affecting the displacement of the particles, such as air drag.

7 Possible Applications

In the past, the modal phenomenon of Chladni patterns mainly influenced areas of art with its complex and dynamic features. Recently, however, the properties of Chladni patterns have been exploited to create new sorting mechanisms (even on the scale of nanoparticles) that might have scientific and industrial applications. Dorrestijn et al. has experimentally proven that this spatial autocorrelation phenomenon can be used as a size-based sorting mechanism: nanoparticles are moved toward either the nodes or the antinodes, based on their size [5]. In my study, I have presented possible methods of area-based and particle-damping-based sorting mechanisms. These mechanisms can be collectively used to sort particles, organelles, or cells. Dorrestijn et al. also suggested the use of such systems in patterning applications, where particles can be fixed using laser curing or photo-polymerization [5]. Once the particles have attained the desired position, the liquid can be removed, and then the patterns can be transferred to a chip surface by nanotranfer printing [17, 18]. All numerical simulations in this study were performed on a $10m \times 10m$ oscillating plate; this presents new possibilities of using Chladni patterns in large-scale applications such as industrial processes.

Perhaps one of the most promising applications of this research could be in sorting cancer cells. Suresh studied the biomechanical characteristics that differentiate mutated cells from benign cells. Recent findings show that lung, breast, and pancreatic metastatic cells are 70% softer than benign cells [19]. Such distinctive elastic properties can be utilized with the particle-damping sorting mechanism (see Section 6.2) to effectively separate cancer cells from normal cells. Researchers have also found correlations between various stages (intensities) of cancer and the biomechanical properties of the affected cells [20]. Hence, sorting mechanisms cannot only be used in the identification but also in the classification of various stages of cancer, which might be helpful in monitoring the progress of treatments. Using Chladni patterns as a sorting system is highly advantageous because it requires minimal data analysis and it uses simple, cost-effective equipment. However, further detailed investigations are necessary to confirm sorting mechanisms using Chladni patterns.

8 Conclusion

In this study, I have presented both quantitative and qualitative effects of adhesive, frictional, and damping forces on Chladni patterns. The friction-based surface displacement model effectively predicted the position of a particle accelerating toward an antinode. The ejection-area model successfully replicated the region in which particles broke away from the surface, despite the adhesive force. Both the area-based and the particle-damping-based sorting mechanisms effectively separated particles that have distinct characteristics. In addition, the results of the spatial autocorrelation analysis were consistent with the models of Chladni patterns studied here. In future, these models should be experimentally verified, and external factors such as air drag, temperature, and deformations of the plate and particles should be investigated.

References

[1] D. Ullmann. Life and work of e.f.f. chladni. *The European Physical Journal - Special Topics*, 145:27, 2007. 10.1140/epjst/e2007-00145-4.

[2] C. Gough. The violin: Chladni patterns, plates, shells and sounds. *The European Physical Journal - Special Topics*, 145:77–101, 2007. 10.1140/epjst/e2007-00149-0.

[3] H. Gerner, M. Hoef, D. Meer, and K. Weele. Inversion of chladni patterns by tuning the vibrational acceleration. *Phys. Rev. E*, 82:012301, Jul 2010.

[4] Henk Jan van Gerner. *Newton vs Stokes : competing forces in granular matter.* PhD thesis, Enschede, April 2009.

[5] M. Dorrestijn, A. Bietsch, T. Açıkal ın, A. Raman, M. Hegner, E. Meyer, and Ch. Gerber. Chladni figures revisited based on nanomechanics. *Phys. Rev. Lett.*, 98:026102, Jan 2007.

[6] R. Thomas. Chladni's law for vibrating plates. *American Journal of Physics*, 50:271–274, March 1982.

[7] Lenoard Meirovitch. *Analytical Methods in Vibrations.* Prentice Hall, 1967.

[8] Wence Xiao. Chladni pattern. Basic studies in Natural Sciences, RUC, May 31 2010.

[9] Micheal Faradray. On a peculiar class of acoustical figures. *Philosophical Transactions*, 121:299–340, January 1 1831.

[10] L. Rayleigh. On a peculiar class of acoustical figures; and on certain forms assumed by groups of particles upon vibrating elastic surfaces. *Philosophical Transactions*, 175:1–21, January 1 1884.

[11] Mary D Waller. Air circulations about a vibrating plate. *British Journal of Applied Physics*, 6(10):347, 1955.

[12] M. Dorrestijn, A. Bietsch, T. Açıkal ın, A. Raman, M. Hegner, E. Meyer, and Ch. Gerber. Chladni figures revisited based on nanomechanics. *Phys. Rev. Lett.*, 98:026102, Jan 2007.

[13] D. A. Griffith. Spatial autocorrelation. University of Texas at Dallas, Richardson, TX, USA, 2009.

[14] H. Wilson, L. Turcotte, and D. Halpern. *Advanced Mathematics and Mechanics Applications Using MATLAB*. Chapman and Hall/CRC, 3 edition, 2003.

[15] Jürgen Tomas. Mechanics of particle adhesion. Mechanical Process Engineering, Department of Process Engineering and Systems Engineering.

[16] S. Ripperger and K. Hein. Measurement of adhesion forces in air with the vibration method. *China Particuology*, 3(1-9), 2005.

[17] T. Kraus, L. Malaquin, E. Delamarche, H. Schmid, N. D. Spencer, and H. Wolf. Closing the gap between self-assembly and microsystems using self-assembly, transfer, and integration of particle. *Advanced Materials*, 17:2438–2442, 2005.

[18] S. Hur, D. Khang, C. Kocabas, and J. Rogers. Nanotransfer printing by use of noncovalent surface forces: Applications to thin-film transistors that use single-walled carbon nanotube networks and semiconducting polymers. *Applied Physics Letters*, 85(5370):3, July 30 2004.

[19] S. Cross, Y. Jin, J. Rao, and J. Gimzewski. Nanomechanical analysis of cells from cancer patients. *Nature*, 2:780–783, December 2 2007.

[20] A. Ketene, E. Schmelz, P. Roberts, and M. Agah. The effects of cancer progression on the viscoelasticity of ovarian cell cytoskeleton structures. *Nanomedicine*, June 6 2011.